Application of Dielectric and Fibre Bragg Grating Strain Measurements to Cure Monitoring

There is significant potential for real-time, on-line cure monitoring in the commercial processing of polymer-based materials; such as composites, adhesives and coatings. Dielectrometry, in particular, is one of the most commercially developed techniques available, establishing relationships between changes in real-time dielectric properties and the viscosity and cure state of a resin-based component. The opposite, however, is true for fibre optic sensor technology. A low general awareness, combined with limited exploitation of fibre optic cure monitoring possibilities, has meant this subject remains primarily in the realm of academic research.

This Measurement Note provides an evaluation of the performance of both dielectric and fibre optic strain methods used to assess the state-of-cure of thermosetting polymers. Particular emphasis is placed on detailing the experimental techniques, requisite equipment, benefits and limitations and the requirements for extending the method into an industrial manufacturing environment.

Both techniques proved valuable in monitoring cure, showing sufficient sensitivity to detect aged materials and post-cure reaction, although dielectrometry was generally more robust, cost effective and provided the most detailed cure information of the two methods.

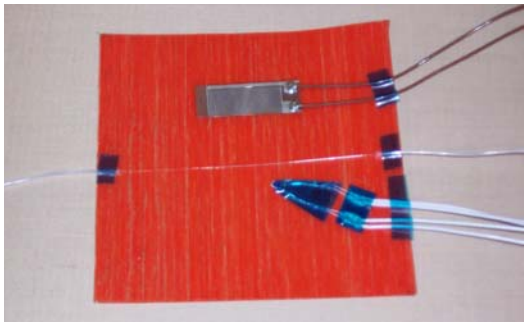

M J Lodeiro and M G Cain

August 2003

INTRODUCTION

Cure monitoring is a means of tracking the changes in physical state or chemical reaction that occur during the processing of many polymeric materials. There is a large prospective industrial market for real time, on-line cure monitoring in the processing of thermosetting polymer-based materials. The aim is to reduce manufacturing variability and costs, whilst simultaneously increasing production rates and component acceptability.

The "cure" of thermoset polymers is a process that converts a liquid resin mixture into a solid by means of chemical reactions, often activated by heat. As cure progresses, there is an increase in molecular weight accompanied by an increase in viscosity, until eventually the system "gels" (is no longer able to flow) and finally "vitrifies" (material T_g rises above the cure temperature).

The two cure measurement techniques considered in this study are:

- fibre optic strain sensing, and
- dielectric.

The adoption of optical fibre methods is hampered by a low general awareness of these techniques and the perceived expense and complexity of the equipment and information processing required. Optical fibre methods can be broadly split into 3 groups [1], based on the resin characteristics which are monitored:

- spectroscopy (FTIR & Raman) - changes in the concentration of specific reactive resin species,
- optical property measurement - changes in the refractive index or fluorescence of the resin, and
- mechanical property measurement (Bragg gratings) - changes in internal resin strain.

Material strain measurement using optical fibre Bragg gratings is the most developed of the optical cure monitoring methods. This is primarily due to the surge in interest and adoption of structural health monitoring, where gratings are applied to structures usually for in-service applications. The evolution of strain as a means of determining cure progress has not been widely investigated, even though there is increased research into processing-induced residual strains [2].

Dielectrometry [3], on the other hand, is the most commercialised of all the cure monitoring methods, and is purportedly the most comprehensive at detecting all important stages during cure:

- resin flow,
- minimum viscosity,
- gelation, and
- vitrification.

Despite this, industrial adoption has been limited, possibly due to the seemingly abstract nature of dielectric properties from the viewpoint of material processors and engineers, combined with uncertainty in the relationship with relevant processing parameters.

Both the electrical and optical techniques require probes or sensors to be embedded within or, at least, to remain in intimate contact with the component during processing. It is possible however, for electrical sensors to be mounted on the outer surfaces of a component or to be integrated into a mould tool wall. The optical sensors can be used for subsequent structural health and lifetime monitoring of a component.

The aim of the work presented here was to evaluate the performance of both methods for their effectiveness in assessing the state-of-cure of thermosetting polymers and investigate their applicability to industrial manufacturing processes.

FIBRE BRAGG GRATINGS

This technique uses optical fibres embedded in the resin to monitor the accumulation of strain within the material, due to constrained thermal deformation and chemical shrinkage during cure.

Background

Optical fibres are waveguides used to confine light. They usually consist of silica glass cores surrounded by cladding of a lower refractive index. As a result, total internal reflection occurs at the boundary and light propagates along the fibre core. The typical structure is shown in Figure 1. Additional polymer layers provide damage protection.

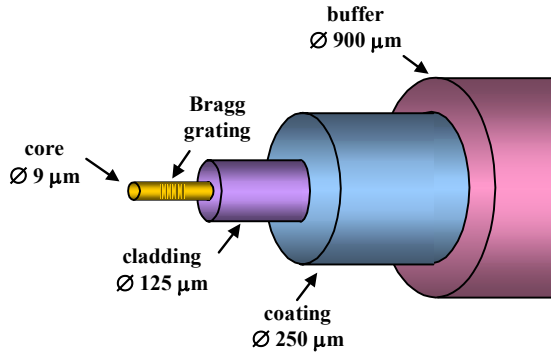

Figure 1 - Basic structure of optical fibre with Bragg grating.

A Bragg sensor is a segment of optical fibre with a longitudinal periodic modulation in the core refractive index [4] which acts as a narrowband reflection filter. These segments are typically 3-15 mm long.

The basic principle of operation is the measurement of changes in the wavelength of the reflected signal, i.e. centre or Bragg wavelength, when illuminated with a broadband light source. This is shown schematically in Figure 2.

The Bragg wavelength is dependent on the effective refractive index of the core, n_{eff}, and the grating periodic spacing, Λ.

Theory

The Bragg wavelength, λ_B, can be expressed as [5]:

$$\lambda_B = 2\, n_{eff}\, \Lambda$$

consequently any external factors, i.e. mechanical strain, $\Delta\varepsilon$, or temperature, ΔT, which act to alter the characteristic grating properties can cause a shift in the reflected wavelength.

For a 'free' fibre this wavelength shift can be expressed:

$$\Delta\lambda_B = \lambda_B \left(K\Delta\varepsilon + \beta\Delta T \right)$$

where K is the wavelength-strain sensitive factor (typically 1 pm/microstrain) and β is the wavelength-temperature sensitive factor (typically 10 pm/°C). Hence the influence of temperature is 10 times more significant than the effect of strain and so temperature compensation is critical for accurate strain determination.

These factors can be reduced further to:

$$K = 1 - p_e$$
$$\beta = \alpha_\Lambda + \zeta$$

where p_e is an effective strain-optic constant and $1\text{-}p_e$ is termed the gauge factor of the grating; α_Λ is the thermal expansion coefficient of the fibre/grating and ζ is the thermo-optic coefficient.

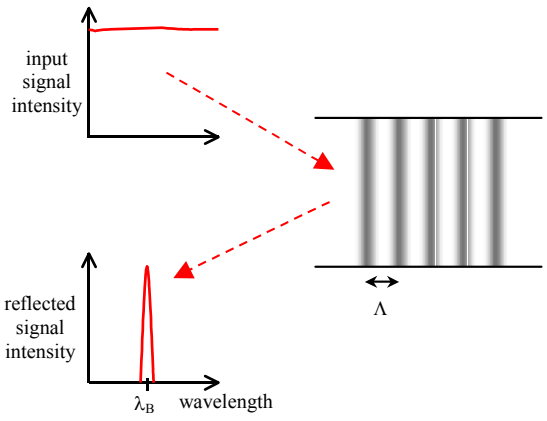

Figure 2 - Typical spectral response of a fibre Bragg grating.

In simplified terms, these factors make corrections to account for the following:

- strain-optic constant, p_e, - effect of mechanical strain on refractive index,
- thermal expansion coefficient, α_Λ, - effect of thermally induced strain on the grating period, and
- thermo-optic coefficient, ζ, - effects of both the thermal strain and the temperature on the refractive index.

Thus the measurement of changes in the Bragg wavelength incorporates the linear effects of the imposed strain, due to both mechanical and thermal expansion, and the effects of the non-linear properties of refractive index.

A 'constrained' fibre, i.e. one which is embedded within a material, behaves as a 'free' fibre but with an additional contribution from the thermal expansion of the surrounding material. Hence, for a 'constrained' fibre:

$$\Delta\lambda_B = \lambda_B [K \Delta\varepsilon + \beta \Delta T + K (\alpha_s - \alpha_\Lambda) \Delta T]$$

where α_s is the coefficient of thermal expansion of the substrate or host material.

Instrumentation and Implementation

The specifications for the fibres and Bragg gratings, supplied by Advanced Optic Solutions GmBH, used in this exercise were as follows:

- Corning SMF 28 fibre - 6 mol% GeO doped silica core,
- centre wavelength 1306 - 1308 nm,
- grating length 12 mm,
- reflectivity >90%,
- reflected spectrum FWHM <0.3 nm,
- standard bare fibre 9 μm core, 125 μm cladding and 250 μm acrylate recoated,
- 0.5 m pigtails (fibre lengths either side of the grating),
- nominal K of 0.805 /strain,
- nominal α_Λ of 0.55×10^{-6} /°C, and
- nominal ζ of 6.1×10^{-6} /°C.

Individual fibres were attached to single-mode fibre patchcords with integrated angled-face APC-style end-connectors, using a Fujikura FSM 40S arc fusion auto-splicer. Fibre ends were stripped, cleaned and cleaved flat for subsequent joining. The fused area was then protected with a heat-shrink metal reinforced support. Connector surfaces were kept covered when not in use to protect them from deleterious scratches and dirt.

An ElectroPhotonics Corporation FLS 3100 interrogation module was used to illuminate the Bragg grating and to monitor the reflected wavelength via the fibre end-connector. Equations, supplied with the unit calibration certificate, were used to convert the output voltage response into the corresponding wavelength. The signal was subsequently displayed and collected real-time (5 second intervals) on a PC via a National Instruments data acquisition card.

Temperature compensation

A 1/3 DIN PT100 thin film platinum resistance thermometer (PRT) was used to monitor temperature. This provided a good combination of size (2 × 2.3mm), cost, thermal range and response, accuracy and cable/noise compensation when used in a 4-wire bridge configuration. The PRT was monitored using an Automated Systems Laboratory Ltd F250 Precision Digital Thermometer, the analogue output from which was monitored concurrently with the Bragg grating.

The PT100 conversion equation from temperature, T, to resistance, R_T, for $T > 0$ °C is:

$$R_T = R_0 (1 + 3.9083 \times 10^{-3} T - 5.775 \times 10^{-7} T^2)$$

This gives a conversion constant of roughly 0.385 Ω/°C, where R_0 is the measured resistance at 0 °C (nominally 100 Ω for a PT100).

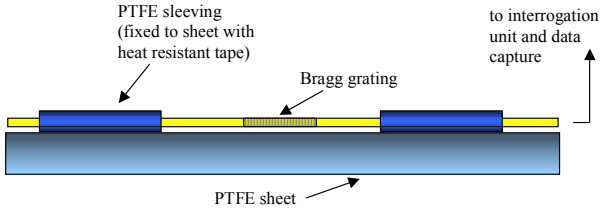

Figure 3 - Set-up for determining β coefficient and strain noise.

Experimental checks

Experiments were run to:

- evaluate the true wavelength-temperature sensitive factor, β (literature value of β is 6.65×10^{-6} /°C), and
- determine the noise limited strain resolution.

These were carried out with a freely supported fibre Bragg grating placed inside a programmable, sensor controlled, air circulation oven, as shown in Figure 3. A PRT was mounted adjacent to the grating to monitor the local temperature.

Three separate heating cycles were performed:

- 2 °C/min to 115 °C followed by natural fan-assisted cooling,
- 5 °C steps to 100 °C, 30 min dwell per step, and
- constant 30 °C.

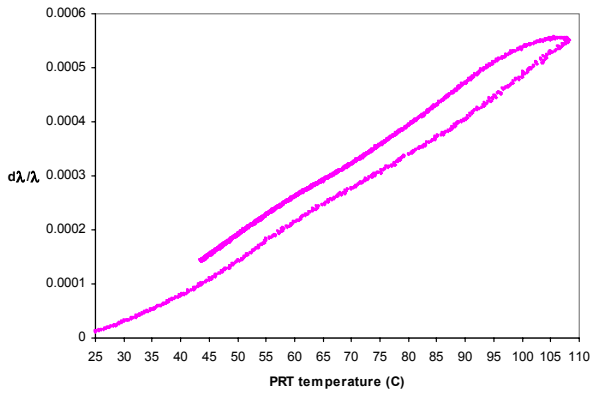

Figure 4 - Bragg response to ramped heating and cooling.

The dynamic heating cycle resulted in a temperature lag between the instantaneous oven temperature, as measured by the PRT, and the internal fibre temperature. This was demonstrated by the displacement between the heating and cooling portions of the cycle, as shown by the graph in Figure 4. Taking an average of the heating and cooling slopes gives an estimate of 6.844×10^{-6} /°C for β.

The staggered heating cycle was designed to ensure thermal equilibrium was achieved. This was verified by the wavelength plateaus shown in Figure 5. Averaging the wavelength and temperature data of the plateaus enabled the β coefficient to be calculated, as shown in Figure 6, giving a value of 6.831×10^{-6} /°C.

This final value was used for all subsequent temperature corrections to the Bragg wavelength.

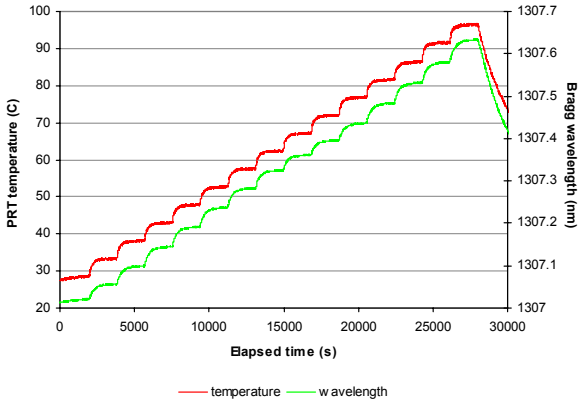

Figure 5 - PRT temperature and Bragg wavelength response to stepped heating.

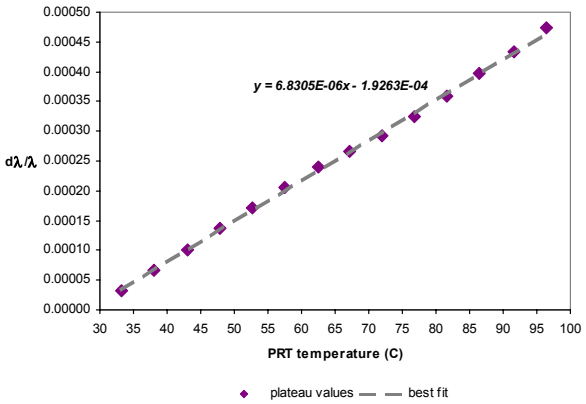

Figure 6 - Plot of plateau values of both wavelength and temperature for β evaluation.

Small fluctuations in temperature and wavelength were observed during the constant temperature cycle. Following wavelength corrections due to temperature variation, the minimum practical strain resolution was found to be around 2 µstrain, as shown in Figure 7.

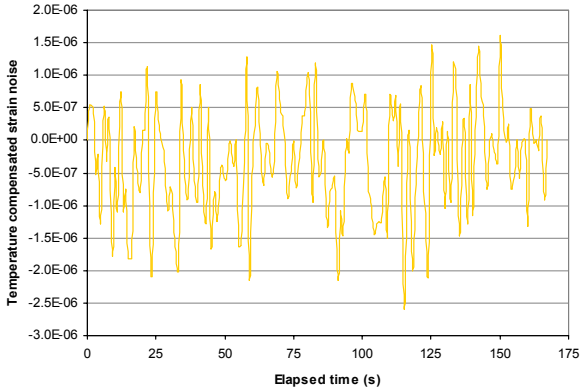

Figure 7 - Typical fibre Bragg grating strain noise.

Sensor integration and measurements

Initially, tests were carried out on HexPly 913 unidirectional glass/epoxy composite, both in-life and out-of-date (5 years). This was laid up 20 plies thick with fibre Bragg gratings included on the mid-plane, at both 0° and 90° orientations with respect to the principal reinforcing fibre direction. Sections were cut-out from the central 6 plies to accommodate narrow bore PTFE tubing, used to protect the fibre where it exits the material. This arrangement is shown schematically in Figure 8. A PRT was positioned close to the grating for temperature correction. These laminates were vacuum consolidated and cured (2 °C/min to 120 °C, 4 hr dwell) in an air circulating oven.

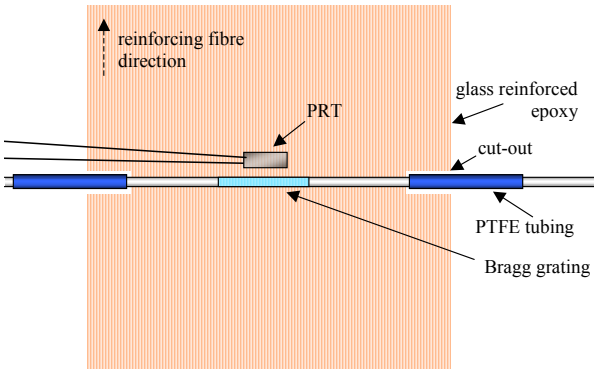

Figure 8 - Mechanism for fibre inclusion, shown for 90° orientation.

Results

Results from the initial Bragg grating tests on orientation are presented in Figures 9 and 10. These show:

- compressive strain changes are observed close to 120 °C which are likely to be related to cure shrinkage,
- greater strain changes in 90° than 0° direction due to restrictions on cure shrinkage imposed by reinforcing fibres,
- clear strain changes occur between 1:12 and 2:24 for the 90° orientation, the strain rate slowing with time eventually reaching a plateau, and
- early changes in strain possibly due to

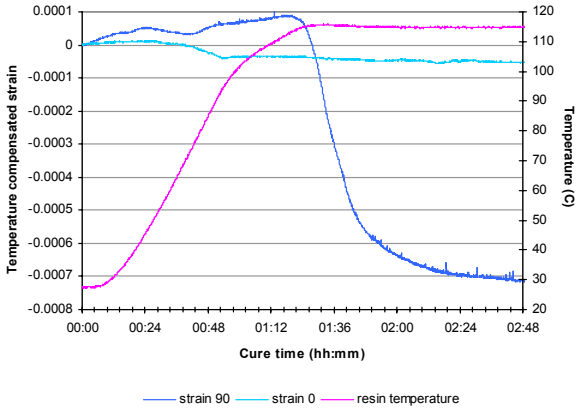

Figure 9 - Plot of temperature & strain with time for both 0° and 90° Bragg gratings.

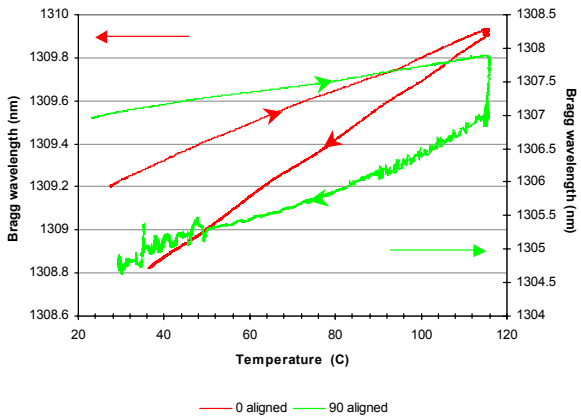

Figure 10 - Plot of Bragg wavelength with temperature for 0° and 90° Bragg gratings.

fibre optic relaxation and/or changes in material thermal expansion and viscosity.

Results from the aged material tests are shown in Figures 11 and 12. These show:

- large relaxation of pre-tension strain as resin viscosity drops,
- greater accumulation of cure shrinkage strain in current than in out-dated material suggesting greater degree of cure,
- shrinkage initiating at a slightly lower temperature for the in-life material,
- cure shrinkage finishing earlier in out-of-date than in-life material possibly suggesting an incomplete cure reaction or a lesser degree of cure is attained, and
- repeats in Figures 9 (90°) and 11 (in-life) have similar shrinkages, measured from gel point, of ~ 0.0008 compressive strain.

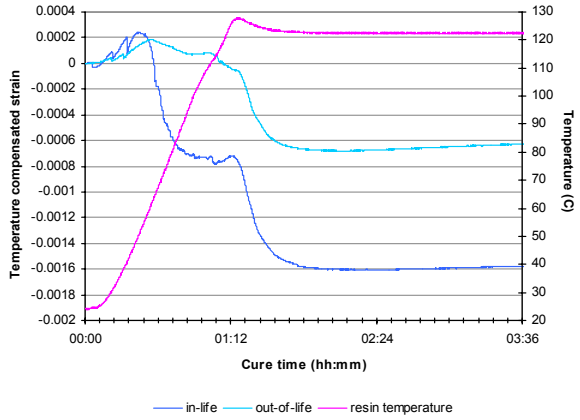

Figure 11 - Plot of temperature & strain with time for both in-life and out-of-date Hexply 913 glass.

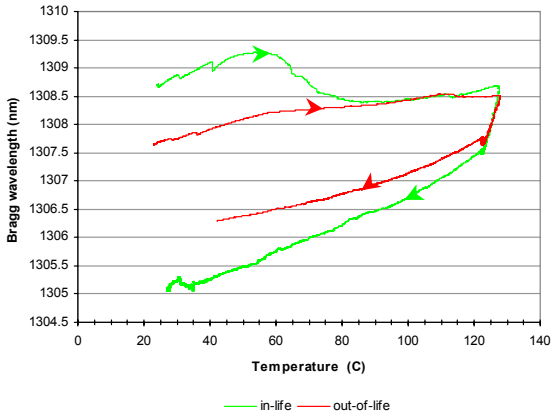

Figure 12 - Plot of Bragg wavelength with temperature for in-life and out-of-date Hexply 913 glass.

Notes

- Bragg grating cure sensors are not re-usable, as they remain embedded within the final product.
- Sensors have greater sensitivity to cure shrinkage when aligned perpendicular to the principal reinforcement direction.
- Sensible precautions should be taken to ensure that neither the resin constituents nor the processing conditions are detrimental to the fabric of the fibre optic.
- Fibre pre-tension, bends and applied vacuum/compaction pressure complicates the cure shrinkage strain profile.
- Fibre optic sensors are fragile at the resin exit point due to the stiffness mismatch and require reinforcement in this region.
- Tight radii of curvature in fibre optics result in signal loss and are best avoided.
- Bragg gratings can be located along a length of fibre optic by their enhanced colouration and increased surface roughness.
- For the most accurate measurements, β should be measured independently for each fibre.
- Pressure also affects the Bragg wavelength, although the effect on the resin is likely to be far greater than that on the grating.

Recommendations

Fibre optics have great potential for cure monitoring. They exhibit high sensitivity to cure shrinkage, as well as a host of external factors whose effects should be minimised. Therefore, a significant level of expertise is required in their handling and interpretation.

This technique has a natural affinity for composite material manufacture where high sensor and instrumentation costs are easily accommodated in low volume, high value product industries. However, the method shows even greater sensitivity in isotropic polymers. The technique is most efficiently used where subsequent structural health monitoring is a benefit.

Problems arise in practice due to the fragile nature of the sensor. Cabling requirements may cause difficulties in closed-mould/high pressure processes or continuous lines.

DIELECTROMETRY

This technique uses electrodes in contact with the resin to monitor the evolution of the intrinsic electrical properties of the material, occurring due to chemical and physical changes during cure (viscosity and T_g).

Background

The basic principle of operation is the measurement of changes in the voltage and current between a pair of electrodes [3].

The application of a sinusoidal voltage to a pair of electrodes creates a localised electric field. This induces ion motion and dipole rotation within the resin generating a sinusoidal current. These motions are hindered by viscous drag, resulting in a phase difference between the applied voltage and the stimulated current, as shown in Figure 13.

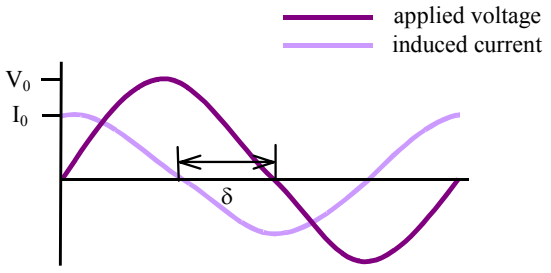

Figure 13 - Amplitude and phase relationship between applied voltage and current response.

This charge redistribution and reorientation only occurs whilst the charged species are sufficiently mobile to respond within the timescale/frequency of the exciting field. By measuring the current and associated voltage at regular intervals and several frequencies as cure progresses (as wide a range as possible within 10^{-4} - 10^{11} Hz); the changing conductance and capacitance of the resin can be determined.

The electrical properties may be expressed in different ways, from the measured voltage, V_0, and current, I_0, and phase shift, δ.

The most basic method is the complex impedance, Z. This defines the a.c. electrical resistance, and thus comprises phase angle information. Z is determined by (' - indicates the "real" part and '' - indicates the "imaginary" part):

$$\mathbf{Z = Z' - i\,Z''}$$

$$\mathbf{|Z| = \sqrt{(Z'^2 + Z''^2)} = V_0 / I_0} \text{ and } \mathbf{Z'' / Z' = \tan \delta}$$

This can be converted to dielectric permittivity, ε, which defines the ability of the material to store charge from the applied field, using [6]:

$$\boldsymbol{\varepsilon = \varepsilon' - i\,\varepsilon''}$$

$$\boldsymbol{\varepsilon' = -Z'' / \omega C_0 Z^2} \quad \text{and} \quad \boldsymbol{\varepsilon'' = -Z' / \omega C_0 Z^2}$$

where $C_0 = \varepsilon_0 A/d$ is the vacuum geometric inter-electrode capacitance of the cell; ε_0 is permittivity of vacuum (8.854×10^{-12} F/m) and A/d is the cell constant which is dependent on the electrode spacing.

Theory

The analysis used in the interpretation of dielectric data depends on the particular behaviour of the material under investigation, which may change between early and later stages of cure, hence:

- dipolar component - dominates at high frequency and high viscosity, such as after gelation, and
- ionic component - dominates at low frequency and low viscosity, such as prior to gelation, as well as at high temperatures.

Equivalent circuits

It is convenient to use electrical circuits made up of resistors and capacitors to represent the electrical characteristics of a resin.

Different equivalent circuits can be used to

describe materials exhibiting particular behaviour [7]:

- relaxation - series circuit (these materials show a peak in ε'' or dielectric loss factor),
- conduction - parallel circuit (these materials show a peak in Z'' or imaginary impedance), and
- relaxation and conduction - combined circuit.

Examples of the expected electrical response for each of these types of material behaviour are presented in Figure 14.

For a resistor, R_S, and capacitor, C_S, in series:

$$\mathbf{Z = R_S + 1 / i\omega C_S}$$

where ω is the angular frequency of the applied field. For a resistor, R_P, and capacitor, C_P, in parallel:

$$\mathbf{Z = (R_P - i\,\omega\, C_P\, R_P^2)/(1 + \omega^2\, C_P^2\, R_P^2)}$$

These model systems are complicated by additional factors, other than charge migration and dipole orientation, when studying real materials [8]:

- electrode polarisation - accumulation of ions at the polymer-electrode interface, and
- interfacial or space charge polarisation - accumulation of charges at boundaries in heterogeneous systems.

Electronic polarisation (displacement of electrons in an atom from equilibrium) and atomic polarisation (deflection of atoms in a molecule from equilibrium) in the presence of an electric field are considered instantaneous effects, forming the minimum background polarisation levels due to an applied field in the frequency range μHz to GHz.

Dielectric permittivity (ε)

For a material showing relaxation, the dielectric permittivity can be described with

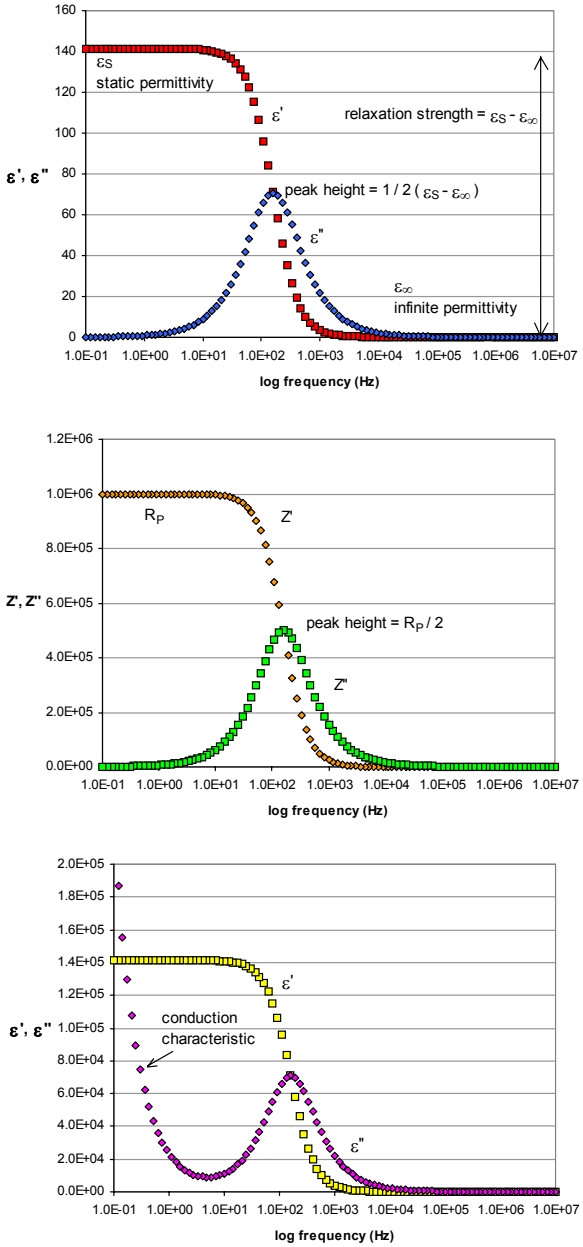

Figure 14 - Typical material responses to an electric field: relaxation (top), conduction (centre) and combined conduction and relaxation (bottom).

the following expression [7] as:

$$\mathbf{\varepsilon(\omega) = \varepsilon_\infty + (\varepsilon_S - \varepsilon_\infty)/(1 + i\omega\tau)}$$

where $\mathbf{\varepsilon_S - \varepsilon_\infty = C_S / C_0}$ and $\mathbf{\tau = R_S C_S}$.

Here, as demonstrated in Figure 14, ε_∞ (at high frequencies) represents the contribution of atomic and electronic polarisation to the dielectric constant, ε', and ε_S (at low frequencies) represents the highest degree of dipole orientation attained for a particular

temperature and field. The relaxation time constant, τ, defines the polarisation decay time upon removal of the exciting field and is a fundamental material property.

Relaxation strength ($\Delta\varepsilon'$)

Another approach is based on the characterisation of the extremes in dielectric constant, ε_∞ and ε_S, or the difference between them, $\Delta\varepsilon'$, which changes systematically during cure at a particular temperature [8].

ε_S is directly related to the material's dipole composition. It increases linearly with degree of cure and decreases with increasing temperature, whereas ε_∞ is independent of these factors.

The primary requirement is a polar nature of either a reactant or one of the products of the cure reaction. In the early stages of cure the decrease in ε' is gradual, with an abrupt drop when the system vitrifies, as shown in Figure 15. ε' should be monitored at a frequency where electrode polarisation is negligible.

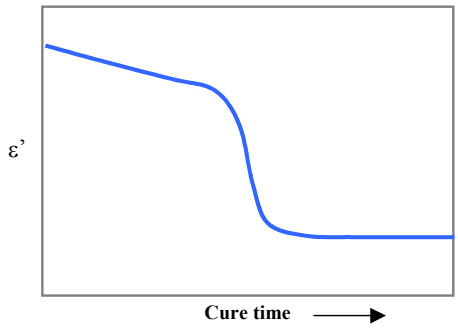

Figure 15 - Evolution of ε' with degree of cure.

Dipole polarisation relaxation time (τ)

The average relaxation time of the curing system increases as the glass transition temperature increases (log τ is proportional to T_g^2) [9]. Consequently the loss peak in ε'', which occurs at a frequency $f_{max} = 1/2\pi\tau$, shifts to lower frequencies with degree of cure under isothermal conditions. Vitrification is assumed when the relaxation time reaches 1 Hz. This method can also be

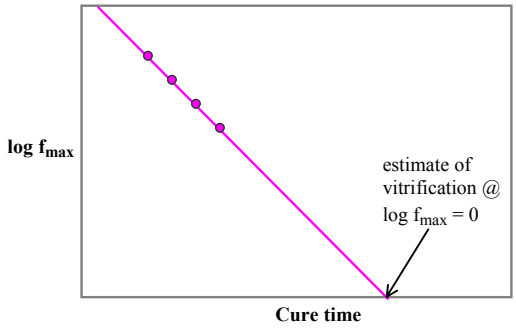

Figure 16 - Change in relaxation time with degree of cure.

used to predict vitrification times by extrapolation, as shown in Figure 16, although subtraction of the ionic contribution may be necessary for this to be successful.

Conductivity (σ)

Charge migration affects the dielectric loss, ε'', adding an extra dissipative contribution such that [10]:

$$\varepsilon'' = (\varepsilon_S - \varepsilon_\infty)\,\omega\tau / (1 + \omega^2\tau^2) + \sigma / \omega\varepsilon_0$$

At frequencies where conduction dominates:

$$\varepsilon'' \approx \sigma / \omega\varepsilon_0$$

Conductivity, σ, is a convenient measure of cure up to the gel point. Prior to the gel point, resin viscosity is inversely proportional to conductivity. Several notable cure stages can be deduced from the conductivity, shown schematically in Figure 17 [11]:

- minimum resin viscosity - corresponds to the maximum in the plot of ionic conductivity with cure time,
- gel point - qualitatively found from point of inflexion on the log conductivity with cure time plot (or the zero slope on the time derivative of the log conductivity, DLIC, or the zero point on the second derivative of conductivity with time, D^2LIC), and
- reaction completion - time derivative of conductivity plotted with cure time is qualitatively similar to the rate of cure such that the plateau region indicates the maximum degree of crosslinking.

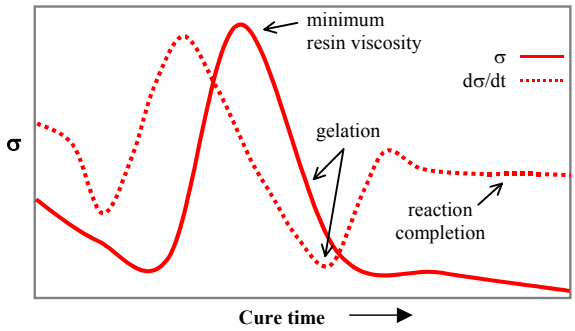

Figure 17 - Typical conductivity–time profile.

Conductivity should be the same for all frequencies if not significantly affected by dipole relaxation (at high frequencies) or electrode polarisation (at low frequencies < 50 Hz). If an apparent frequency dependence is observed then the frequency range of conductivity measurement should be changed to a more insensitive region.

Impedance (Z)

The impedance spectrum can be used in a similar way to the dielectric response of a curing system [12]. For a material showing conduction, the impedance is described as:

$$\mathbf{Z(\omega) = R_P / (1 + i\omega\tau)}$$

where $\tau = R_P C_P$.

The real impedance Z' exhibits dispersion-type behaviour dropping from a maximum plateau value of R_P at low frequency to zero at high frequency, shown in Figure 14.

A plot of the imaginary impedance spectrum, Z'', shows a minimum and a maximum. As cure progresses under isothermal conditions, the values of these minima and maxima increase but shift to lower frequency positions, as shown in Figure 18.

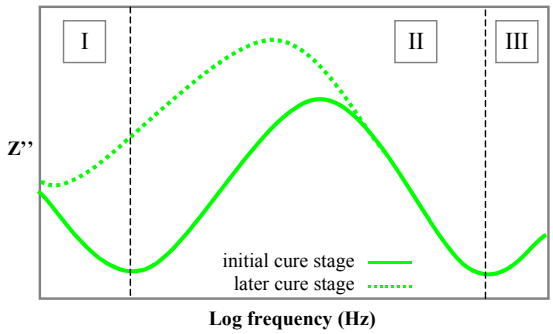

Figure 18 - Typical imaginary impedance profiles at different stages of cure.

This schematic also highlights that the conduction dominated zone at intermediate frequencies (zone II) can be clearly identified from the neighbouring regions dominated by electrode polarisation at low frequencies (zone I) or dipolar relaxation at high frequencies (zone III).

Impedance profiles enable the conductivity to be calculated from the imaginary impedance peak without interference from phenomena which dominate in the adjacent zones, using:

$$\mathbf{Z''_{max} = R_P / 2} \quad \text{and} \quad \mathbf{\sigma = 1/2\, Z''}$$

A plot of log Z'', normalised with respect to the difference between the minimum and maximum values, with time qualitatively resembles a sigmoidal extent of cure trace.

Frequency shift (f_{max} - f_{min})

The combined effects of temperature and material state during dynamic cure can complicate the simple changes in the imaginary impedance profile described in Figure 18. The maximum and minimum both shift to higher frequencies with increasing temperature and to lower frequencies with increasing degree of cure.

The temperature shift for both the maximum and minimum values are similar, but a disparity occurs with the cure-induced shift such that the minimum displays a greater cure sensitivity [13].

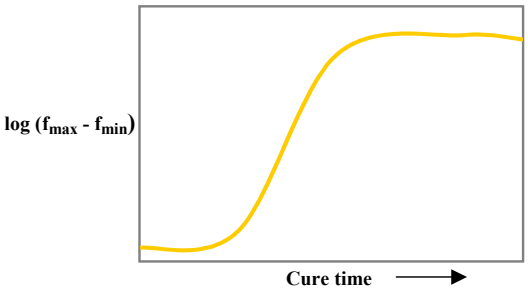

Figure 19 - Change in impedance maxima and minima frequencies with cure.

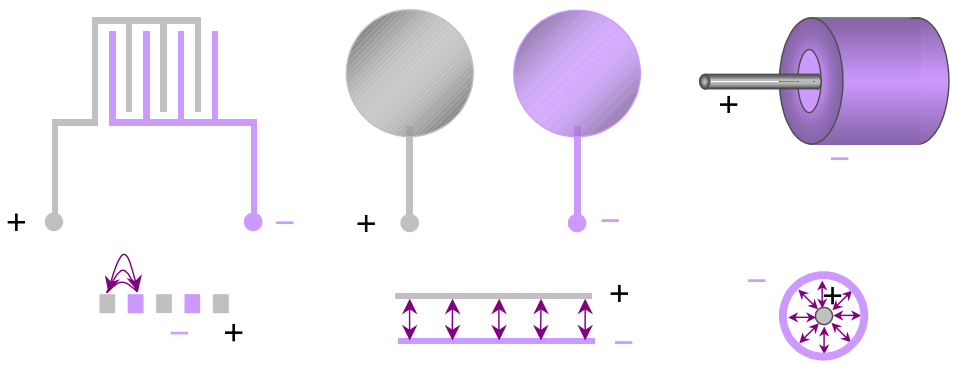

Figure 20 - Basic dielectric sensor configurations and their resultant electric fields: inter-digitated (left), parallel plate (centre) and coaxial (right).

This fact can be used to eliminate the effect of temperature from these observations giving plots of $\log(f_{max} - f_{min})$ with cure time which resemble fractional cure conversion curves. A typical example of this is shown in Figure 19.

Instrumentation and Implementation

Dielectric sensors

There are several electrode configurations available, as shown in Figure 20. The two principal types are:

- inter-digitated sensors, and
- parallel plate or bulk sensors.

Interdigitated sensors are single surface, comb-like metallic electrode patterns printed onto a small, thin insulating substrate layer. They produce localised fringing fields, between adjacent electrode fingers of opposite polarity, extending out into the resin to a distance determined by the electrode geometry/spacing.

Parallel plate sensor pairs are solid areas of metallic electrode deposited onto an insulating base. These produce a uniform electric field between the plates of opposite polarity.

Dielectric sensors can be either implanted or reusable, and positioned for surface or internal measurements. In addition, they need protection from shorting against any conductive components within the material, e.g. metallic particulate fillers or carbon fibre reinforcement, but must still be in intimate contact with the resin.

The specifications of the IDEX 066S/067S sensors, supplied by Netzsch, used in this study were:

- polyimide substrate 400 μm thick,
- nickel inter-digitated electrodes with 115 μm spacing,
- 2.5 × 0.8 cm sensor area, and
- glass fabric filter barrier layer.

A Solartron 1260 impedance gain-phase analyser was used, in conjunction with a Solartron 1296 dielectric interface, to perform the electrical measurements over a wide frequency range and subsequently collect data at regular intervals (approximately every 5 mins) during the cure cycle. The additional interface increased the maximum measurable impedance and the minimum measurable phase angle difference, by comparing all measurements with internal references. However, the measurement cycle time is increased as a result. Unscreened, temperature resistant wires were used to connect the sensors to the impedance analyser.

Temperature effects

The sensors themselves (e.g. electrode substrate material or surface barrier layer) and the associated cabling may contribute to the dielectric measurements on the curing

resin. These offsets should not be problematic provided they remain constant throughout the cure cycle, but often they are influenced by temperature such that the sensor response obscures the material [14]. This temperature dependence can be determined experimentally and where necessary deducted from the cure data.

Figure 21 shows the temperature response for a number of nominally identical sensors and typical resins. In order to assess the temperature sensitivity of the sensors, a k-type thermocouple was used to monitor bare sensors whilst subjected to ramped heating cycles. The plot shows the responses of individual sensors are relatively flat and broadly similar, but differ by several orders of magnitude from the response of either of the resins. From this, the sensors were assumed to contribute negligibly to the electrical properties of the resin and were not corrected for in subsequent tests.

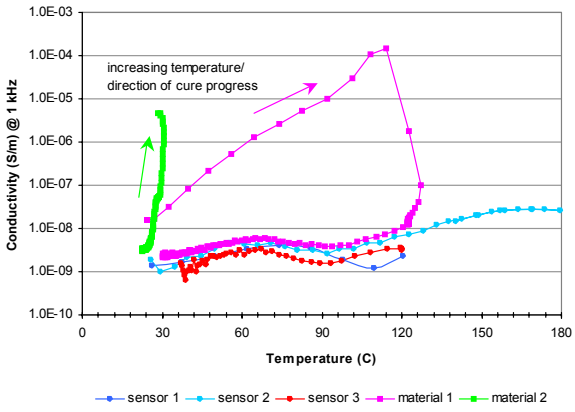

Figure 21 - Temperature dependence of dielectric sensor response.

Experimental checks

Experiments were run to ascertain the most appropriate measurement configuration by comparing the measured output to that expected for a model circuit (parallel R-C), and from a model material (amorphous polycarbonate at 165 °C).

Figures 22 and 23 show selected results. The set-up used in these examples gave the closest response to that expected from both the model circuit and material, with the least

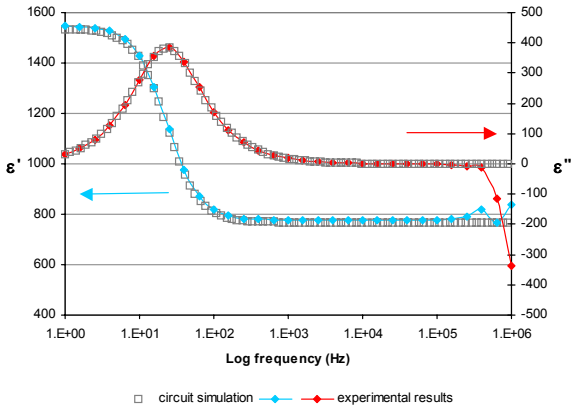

Figure 22 - Dielectric profile produced by parallel R-C circuit.

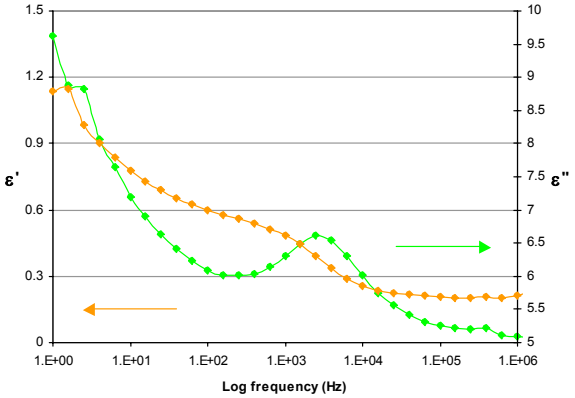

Figure 23 - Dielectric profile from polycarbonate at 165 °C.

noise, and so was used for subsequent cure measurements.

This configuration comprised:

- 1296 dielectric sensor + 1260 impedance analyser using internal reference mode,
- frequency range 1-10^6 Hz ,
- 1 V_{rms} applied exciting field,
- 5 data points/decade (31 points/sweep),
- 3 cycle average per data point, and
- total sweep time ~ 1 min 45 secs.

Sensor integration and measurements

Bare sensors were used for all cases except the conductive materials, where a glass tissue and PTFE coated woven glass screen were

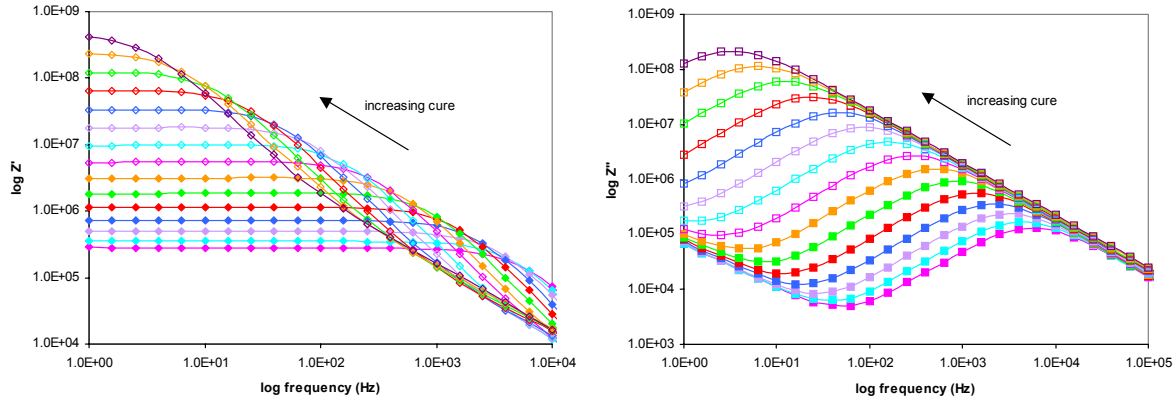

Figure 24 - Real and imaginary impedance profiles during room temperature cure of DP 460 epoxy.

used to cover the electrodes. The sensors were positioned in the central region of the material mid-plane. A k-type thermocouple was placed adjacent to the sensor to monitor the local resin temperature.

Dielectric measurements were made on several materials, shown in Table 1.

Results

Most of the materials displayed conduction behaviour, indicated by Z'' maxima, typical examples of which are presented in Figure 24. These clearly show the expected characteristic changes in plateau level and the peak shift with time for isothermal cure. This response would be modified with dynamic temperature changes.

Examples of typical analyses employing conductivity and its time derivatives, maximum imaginary impedance and normalised imaginary impedance are shown graphically in Figures 25 - 27.

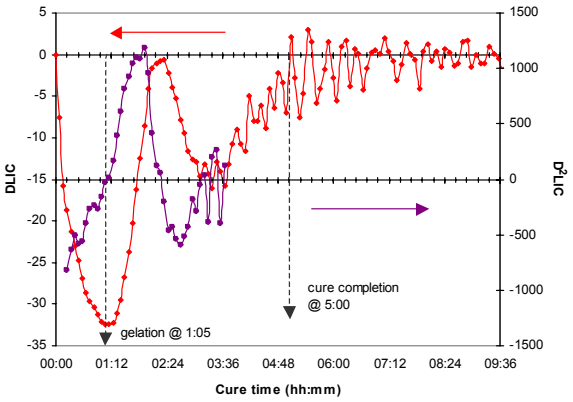

Figure 26 - Time derivatives of log conductivity showing important stages during cure of DP 460.

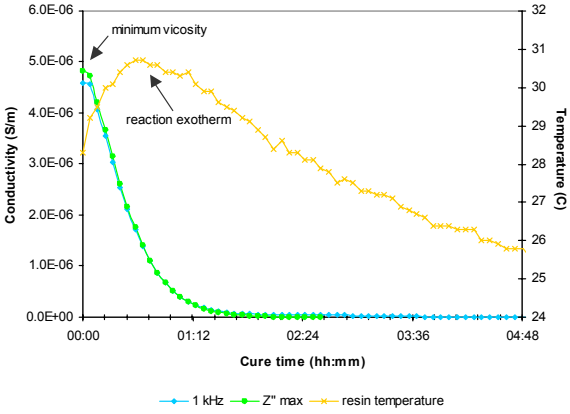

Figure 25 - Independently determined Z'' max and 1 kHz conductivity results for DP 460 cure.

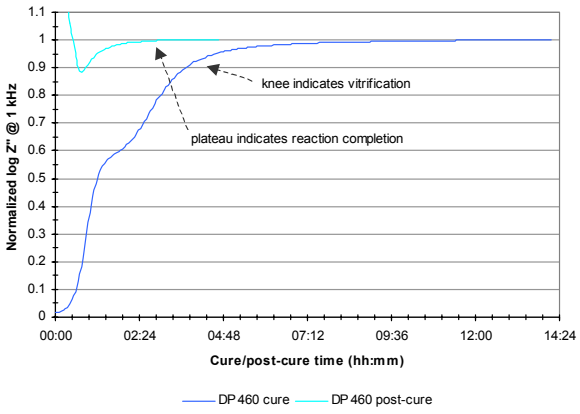

Figure 27 - Normalized imaginary impedance data for DP 460 cure and post-cure.

Table 1 - Materials and cure profiles used in dielectric cure monitoring study.

Material	Format	Cure Cycle
SP Systems SPSE90 biax glass/epoxy pre-preg - fresh & shelf aged	composite laminate 8 plies thick	1°C/min 110°C 5 hour dwell
3M Scotch-Weld DP 460 epoxy adhesive - cure & post-cure	adhesive joint Al adherends	25°C > 12 hour dwell
		1°C/min 100°C 4 hour dwell
Dow Chemicals XD 4601 epoxy adhesive - metal filled	bulk resin 25wt% Cu filings and powder	1°C/min 140°C 8 hour dwell
Hexcel Composites HexPly 924 fabric glass/epoxy pre-preg	composite laminate 10 plies thick	2°C/min 180°C 8 hour dwell

These indicate the important features used to identify different cure events and the interchangeable nature of the Z'' maximum and 1 kHz determined conductivities. However, the Z'' minimum and maximum frequency shift analysis was unsuccessful in all cases.

The results of these analyses for several of the materials are compared in Table 2. Here, the dielectric results compare well with information independently provided by material suppliers. The minimum conductivity after cure does not correspond to the degree of cure merely reaction completion.

The plots in Figures 28 - 30 show the technique has sufficient sensitivity to successfully detect cure stages in high temperature processes, as well as material post-curing and shelf ageing.

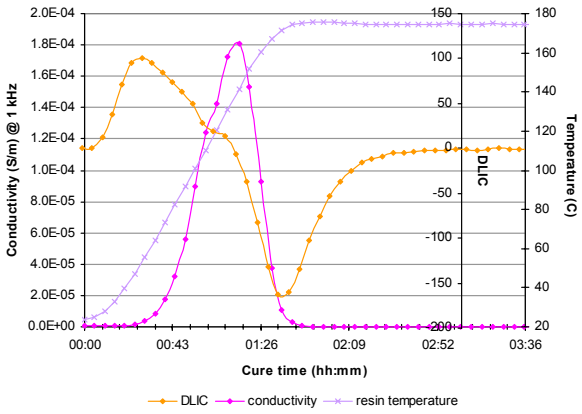

Figure 28 - Conductivity and time derivative of conductivity with cure for HexPly 924 glass.

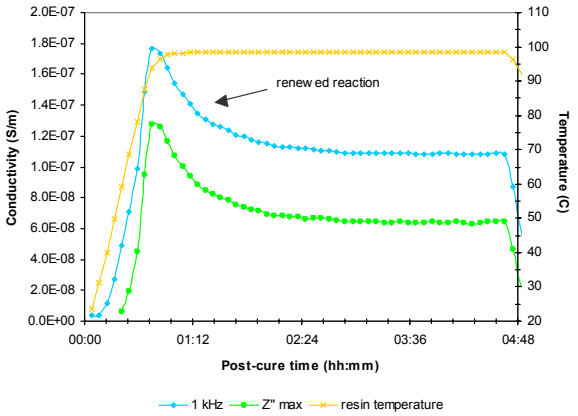

Figure 29 - Conductivity profiles of DP 460 during post-cure.

Table 2 - Detailed cure information from dielectric cure monitoring.

	fresh SPSE90	shelf-aged SPSE90	HexPly 924	DP 460	DP 460 post-cure
minimum viscosity time (hh:mm)	1:30	1:25	1:15	0:00	n/a
minimum viscosity temperature (°C)	103	102	140	n/a	n/a
conductivity @ minimum viscosity (S/m)	3.0×10^{-5}	2.2×10^{-5}	1.8×10^{-4}	4.6×10^{-6}	n/a
gelation time (hh:mm)	1:45	1:40	1:40	1:05	n/a
cure time (hh:mm)	2:50	3:10	3:20	5:00	3:20
conductivity @ cure completion (S/m)	1.6×10^{-8}	7.4×10^{-8}	2.6×10^{-8}	4.3×10^{-9}	1.1×10^{-7}
manufacturer's minimum viscosity temperature (°C)	105		150	n/a	n/a
manufacturer's gelation time (hh:mm)	n/a		1:30	1:00	n/a
manufacturer's cure time (hh:mm)	3:00 (1:10 @ 110°C)		3:20 (2:00 @ 180°C)	24:00	1:50 (1:00 @ 100°C)

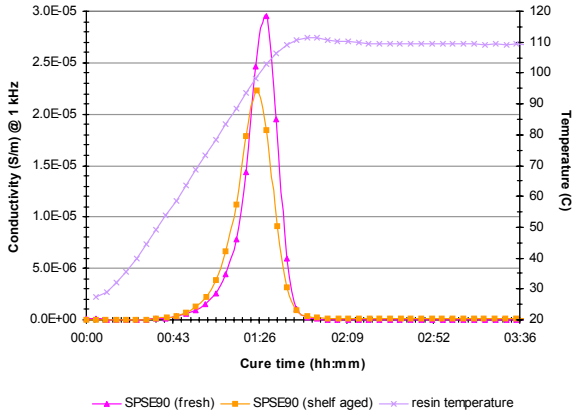

Figure 30 - Different cure conductivity profiles for fresh and shelf-aged SPSE90.

The post-cured DP 460 showed a drop in conductivity with post-cure time suggesting that further charged species were integrated into the polymer network, thus a plateau in conductivity would correspond to vitrification at the higher post-cure temperature.

Differences in the electrical behaviour of the fresh and shelf-aged SPSE90 can be similarly attributed to the mobility of charged species. Minimum viscosity is reached sooner and the conductivity is lower for the aged material, indicating a higher minimum viscosity and less resin flow. Gel occurs earlier and cure times are longer for the shelf-aged material, as might be expected. The conductivity of the aged material is higher at cure completion, possibly due to charged species remaining unreacted and a lower level of cure being achieved.

The metal filled XD 4601 showed no discernable peaks in either ε'' or Z''. This is either due to the particular nature of the resin or due to the effect of metal particles infiltrating the protective fabric layers covering the electrodes and short circuiting the cell. Tests with unfilled resin would confirm this.

Notes

- Although parallel plate sensors offer an average measure of cure through a material; the overlapping areas, alignment and separation of the two electrodes must be tightly controlled for valid results.
- Usually a thin layer of glass fibre fabric, polyimide film or thin porous PTFE peel ply is sufficient to protect electrodes from shorting due to contact with conductive fillers.
- The impedance frequency sweep time must be short enough that the curing system does not change appreciably during the measurement and can be considered instantaneous.
- Often dielectric sensors remain within the cured product and may act as a flaw, therefore re-usable sensors built into mould tool walls are preferred.
- Low applied voltages are required to minimise possible electrochemical reactions.
- Most impedance/dielectric analysers are functionally equivalent and so can be used interchangeably.
- The electric field from a comb sensor extends out into the resin to a distance determined by the electrode spacing.

Recommendations

This technique provides the greatest information as it has at least some sensitivity to all the major stages of cure, but it does require considerable skill and experience on the part of the operator in implementation and interpretation. Large quantities of data are produced and hence there is a great deal of data reduction and analysis necessary.

Unlike many other cure monitoring techniques, it is sensitive both to the effects of ageing in resins and to post-cure in the solid state. The technique is intermediate in sensor and equipment costs, but is unsuitable for high volume/low value production where the added cost per component would be prohibitive.

Cabling requirements hinder easy application to closed-mould processes or continuous high speed lines.

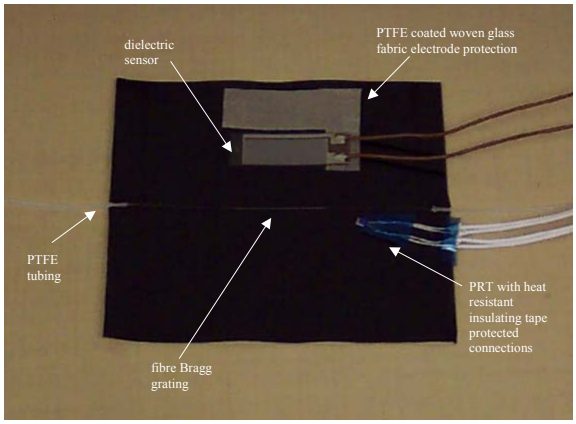

Figure 31 - Typical set-up for dielectric and Bragg cure monitoring in conductive SPSE84.

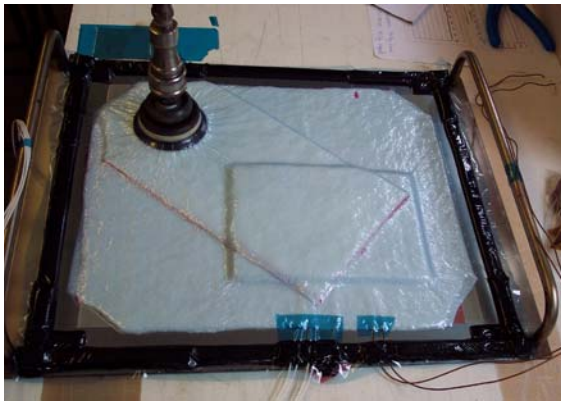

Figure 32 - Typical vacuum bagging/ consolidation of test laminates.

Table 3 - Materials and cure profiles for the comparative study.

Material	Format	Cure Cycle
SP Systems SPSE84 ud carbon/epoxy pre-preg - cure & post-cure	composite laminate 14 plies thick	1°C/min 110°C 6 hour dwell
		1°C/min 150°C 4 hour dwell
Hexcel Composites HexPly 913 ud glass/epoxy pre-preg	composite laminate 20 plies thick	2°C/min 125°C 4 hour dwell

COMPARATIVE STUDY

In addition to individual assessments of dielectric and fibre Bragg cure monitoring, a series of simultaneous monitoring experiments were run to determine the effective correlation of events between the different techniques.

Tests were conducted on the materials listed in Table 3. A typical sensor set-up is shown in Figure 31 and the final vacuum bag sealed laminate is shown in Figure 32.

Results

The results for these experiments are given in Table 4 and Figures 33 - 36.

Table 4 - Detailed cure information from the comparative study.

	cure SPSE84		post-cure SPSE84		HexPly 913	
	DEA	FBG	DEA	FBG	DEA	FBG
minimum viscosity time (hh:mm)	0:50	n/a	n/a	n/a	1:03	n/a
minimum viscosity temperature (°C)	62	n/a	n/a	n/a	114	n/a
conductivity (S/m) or strain @ minimum viscosity	2.7×10^{-2}	n/a	n/a	-	1.6×10^{-4}	n/a
gelation time (hh:mm)	1:12	1:45	n/a	n/a	1:10	1:12
cure time (hh:mm)	2:40	3:45	3:15	plateau not reached	2:25	2:00
conductivity (S/m) or strain @ cure completion	2.2×10^{-2}	-0.0026	3.7×10^{-3}	-	1.5×10^{-8}	-0.0016
manufacturer's minimum viscosity temperature (°C)	98		n/a		122	
manufacturer's gelation time (hh:mm)	n/a		n/a		1:30	
manufacturer's cure time (hh:mm)	3:30		n/a		2:20	

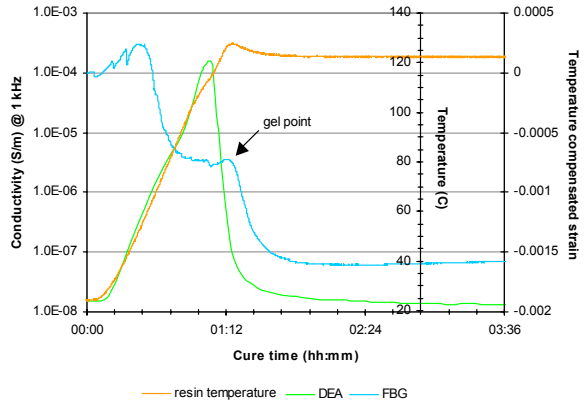

Figure 33 - Dielectric and fibre Bragg cure monitoring of HexPly 913 glass.

Figure 33 shows there is a drop in fibre Bragg grating (FBG) strain with decreasing viscosity. This is most likely to be attributable to the relaxation of pre-tension strain. A close correlation between the development of compressive strain in the fibre Bragg and the onset of gelation as defined by dielectric analysis (DEA) is evident. It can be deduced that the cure shrinkage measured by the fibre Bragg is only measured from the point at which the resin is sufficiently cured/solid that stress transfer between the resin and fibre can occur i.e. at gelation.

Figures 34, 35 and 36 show the FBG and DEA results for a conductive carbon reinforced material. This material displayed relaxation behaviour with peaks in ε'' data. However, these peaks proved difficult to analyse using the various dielectric permittivity routes. These problems may be due to the conductive nature of the reinforcement or the intrinsic nature of the resin, which can be confirmed with unreinforced resin trials. These experiments were therefore analysed using the 1 kHz resin conductivity data. The DEA and FBG profiles for cure are shown in Figure 34, and for post-cure in Figure 35 and 36.

The cure results are more complex than previously seen, with a dip in the conductivity after the minimum viscosity but before cure completion, the cause of which is unclear. Again the decrease in viscosity coincides with a relaxation of the fibre optic pre-tension, but the initiation of cure shrinkage no longer coincides with the apparent gel point. Instead this occurs simultaneously with the sudden step change in conductivity.

This more complex conductivity curve could be due to the creation of charged species as a result of the cure reaction rather than their integration into the polymer network. In this instance, the gel point is more easily distinguished from the fibre optic data than the dielectric results. This may also account for the disparity in cure and gel times between the DEA, FBG and manufacturer's data; since DEA analysis is particularly difficult for this material.

The post-cure DEA results are much more conclusive. These show a clear drop in conductivity as the higher post-cure temperature initiates further reaction beyond the previous level achieved during the

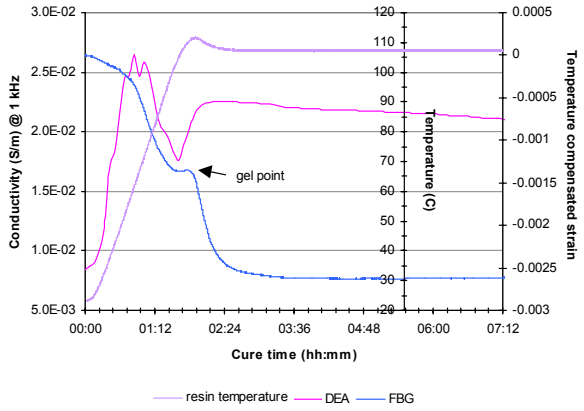

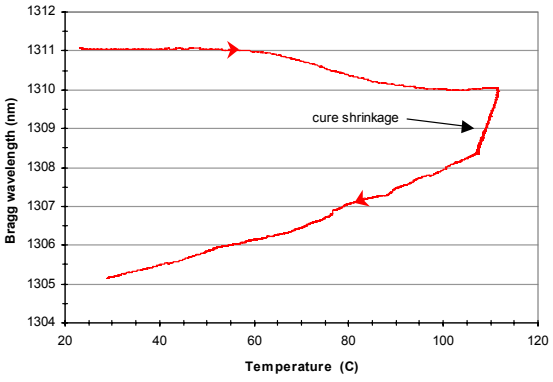

Figure 34 - Dielectric and fibre Bragg cure monitoring of SPSE84 carbon: conductivity and shrinkage strain (left) and Bragg wavelength with temperature changes (right).

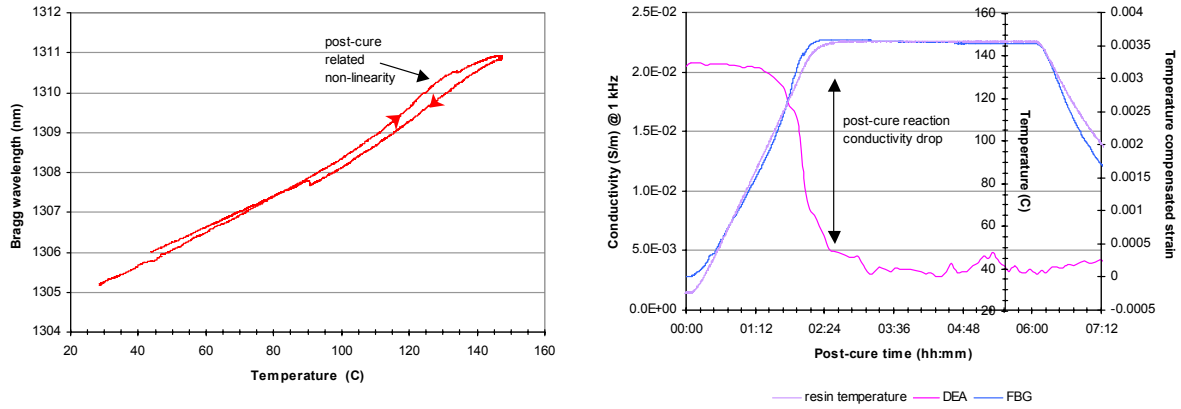

Figure 35 - Dielectric and fibre Bragg post-cure monitoring of SPSE84 carbon: Bragg wavelength with temperature changes (left) and conductivity and shrinkage strain (right).

preliminary cure stage. The FBG data seem less sensitive to this, showing only a small non-linearity in the same temperature region due to the change in the thermal expansion coefficient caused by the increased degree of cure. By magnifying the constant temperature region, as in Figure 36, it can be seen that in fact the FBG data shows a continuing small change in resin strain; either due to additional shrinkage or the development of the final fully cured resin thermal expansion coefficient (CTE).

CONCLUDING REMARKS

Both fibre Bragg and dielectric techniques have successfully shown sensitivity to many of the cure issues which are important to material processors.

Both methods are hampered by mid to high sensor and system costs, variable success in operation and complex/time consuming analysis. Also, inevitably, users will require that the method be correlated empirically with a traditional mechanical/thermal technique for every individual resin system, in order to provide tangible confirmation.

Similarly, all the sensors generally only sample small volumes of material. For fibre Bragg measurements, several gratings can be produced in-line on a single fibre and interrogated individually, in order to extend the measured region. Electrode configurations and spacings can also be modified to increase the sampled material for dielectrometry.

In particular, dielectrometry is effective enough to track the changes throughout cure from liquid to solid states and beyond into post-cure. Whilst the usefulness of dielectrometry is undisputed its application is often difficult, with properties being expressed in different ways leading to confusion in interpreting the same basic data. The distorting effect of conductive fillers on the electric field and subsequent results has not been fully investigated and can itself cause problems in interpretation. However, continuous dielectric chemo-physical sensing holds the most promise for smart, closed-loop processing control.

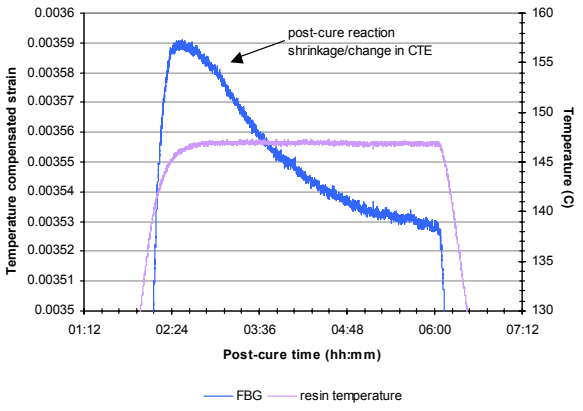

Figure 36 - Magnified view of fibre Bragg HexPly 913 glass post-cure monitoring data.

References

1. *R Davidson and N L Hancox, "Cure Monitoring of Resins in Fibre Composites," AEA Technology Report AEAT – CPD4B – R3, September 2000.*
2. *H Kang, D Kang, H Bang, C Hong and C Kim, "Cure monitoring of composite laminates using fibre optic sensor", Smart Materials and Structures vol. 11, 2002, 279-287.*
3. *T Fukuda and T Kosaka, "Cure and Health Monitoring" Encyclopedia of Smart Materials Volume 1, Ed. Mel Schwartz, John Wiley and Sons, New York, 2002.*
4. *J S Leng and A Asundi, "Real-time cure monitoring of smart composite materials using extrinsic Fabry-Perot interferometer and fibre Bragg grating sensors", Smart Materials and Structures vol. 11, 2002, 249-255.*
5. *M Stewart and M Cain, "NMW0403: Optical Sensor Characterisation and Calibration Device for Integrated Optical Systems", NPL Report MATC(A)57, September 2001.*
6. *F Bellucci, M Valentino, T Monetta, L Nicodemo, J M Kenny, L Nicolais and J Mijović, "Impedance spectroscopy of reactive polymers-1", Journal of Polymer Science B: Polymer Physics vol. 32 (15), 1994, 2519-2527.*
7. *G Williams and D Thomas, "Phenomenological and molecular theories of dielectric and electrical relaxation of materials", Novocontrol Application Note: Dielectrics 3, 1998.*
8. *J Mijović and B Fitz, "Dielectric spectroscopy of reactive polymers", Novocontrol Application Note: Dielectrics 2, 1998.*
9. *G M Maistros and I K Partridge, "Monitoring autoclave cure in commercial carbon-fibre/epoxy composites", Composites Part B vol. 29B (3), 1998, 245-250.*
10. *J Mijović, J M Kenny, A Maffezzoli, A Trivisiano, F Bellucci and L Nicolais, "The principles of dielectric measurements for in-situ monitoring of composite materials", Composites Science and Technology vo.l 49, 1993, 277-290.*
11. *A McIlhagger, D Brown and B Hill, "The development of a dielectric system for the on-line cure monitoring of the resin transfer moulding process", Composites Part A vol. 31A (12), 2000, 1373-1381.*
12. *F Bellucci, M Valentino, T Monetta, L Nicodemo, J M Kenny, L Nicolais and J Mijović, "Impedance spectroscopy of reactive polymers-1", Journal of Polymer Science B: Polymer Physics vol. 32 (15), 1994, 2519-2527.*
13. *A A Skordos and I K Partridge, "Impedance cure and flow monitoring in the processing of advanced composites", International Conference for Manufacturing of Advanced Composites ICMAC, 2001, Belfast UK, 103-112.*
14. *M B Buczek and C W Lee, " Considerations in the dielectric analysis of composites", 40th International SAMPE Symposium, 1995, California USA, 696-710.*

Acknowledgements

The research reported in this Measurement Note was carried out by NPL, as part of the 'Measurement of Materials Systems Programme', funded by the UK Department of Trade and Industry. The authors would like to acknowledge the contributions of colleagues at NPL, in particular, Colin Campbell (fibre optics), Nick McCormick (Bragg gratings), Richard Shaw (composites) and David Mulligan. Thanks are also due to staff at Solartron Analytical, Netzsch and AOS Fibres for their kind assistance.

For further information contact:

Maria J. Lodeiro
NPL Materials Centre
National Physical Laboratory
Queens Road
Teddington
Middlesex
TW11 0LW
Telephone: 020-8977 3222 (*switchboard*)
Direct Line: 020-8943 6034
Facsimile: 020-8943 2989

E-mail: maria.lodeiro@npl.co.uk
Website: http://www.npl.co.uk/npl/cmmt/cure/